

Combining dynamical-decoupling pulses with optimal control theory for improved quantum gates

Matthew D. Grace*

*Department of Scalable & Secure Systems Research (08961),
Sandia National Laboratories, Livermore, CA 94550*

Jason Dominy[†]

*Program in Applied & Computational Mathematics,
Princeton University, Princeton, New Jersey 08544*

Wayne M. Witzel[‡]

*Department of Advanced Device Technologies (01425),
Sandia National Laboratories, Albuquerque, NM 87185*

Malcolm S. Carroll[§]

*Department of Photonic Microsystem Technologies (01725),
Sandia National Laboratories, Albuquerque, NM 87185*

(Dated: June 22, 2022)

Constructing high-fidelity control pulses that are robust to control and system/environment fluctuations is a crucial objective for quantum information processing. Using the two-state Landau-Zener model for simulations of a double quantum dot qubit, we generate optimal controls for π - and $\pi/2$ -pulses, and investigate their inherent robustness. We find enhanced robustness through a novel combination of recent results from dynamical-decoupling and optimal control of unitary operations. Previous work has shown that general errors up to (but not including) third order can be removed from π - and $\pi/2$ -pulses without concatenation. By systematically integrating methods from dynamical-decoupling and optimal control, and incorporating system parameter estimates, we demonstrate, via a numerical example, that gate fidelity may further be improved.

* Electronic address: mgrace@sandia.gov

[†] Electronic address: jdominy@math.princeton.edu

[‡] Electronic address: wwitzel@sandia.gov

[§] Electronic address: mscarro@sandia.gov

I. INTRODUCTION

Demanding requirements for fidelity of gates to achieve fault-tolerant quantum computation (QC) [1] have motivated the need for improved quantum control protocols (QCPs). In quantum information science, there are (at least) three distinct approaches to improving fidelity of qubit operations in the presence of environmental interactions: dynamical decoupling (DD) [2], optimal control (OC) [3], and quantum error-correction (QEC) [1]. In this work, we show that a combination of DD and OC pulse-shaping criteria can be used to produce (a) improved fidelity compared to DD pulses alone and (b) improved robustness to uncertainty in the strength of an environmental perturbation strength, to which the pulses were tuned using OC. For brevity, we refer to this combination of DD and OC as “DD+OC”.

During the past few years, S. Pasini, G. Uhrig, and colleagues have made significant contributions toward the analysis and design of optimal DD pulses for controlling qubits and decoupling them from the surrounding environment, e.g., Refs. [4–8]. In one of their recent articles, they derive control-field criteria to eliminate first- and second-order errors from $\pi/2$ - and π -pulses resulting from qubit-environment interactions [7]. We adapt these criteria for the case of closed-system unitary control, with an environmental perturbation term in the qubit Hamiltonian. Next, we combine these criteria with a novel OC procedure for unitary control that incorporates estimates of the environmental perturbation term to increase the fidelity of these control fields. The DD+OC combination is more robust to uncertainty in the estimated perturbation strength than OC alone. To illustrate the utility of our approach, we optimize and evaluate these controls fields using a general qubit model based on the two-level Landau-Zener Hamiltonian [9]. Related work on hybrid QCPs includes that by Borneman *et al.*, who have recently used OC to design robust control fields to improve the performance of the so-called Carr-Purcell-Meiboom-Gill pulse sequence [10].

The primary objective in this work is to construct a hybrid QCP, combining methods and results from theories of dynamical decoupling and optimal control (OC) to locate control fields that produce high-fidelity rotations about particular axes (e.g., x - or z -axis), which are robust with respect to uncertain, but estimated (i.e., characterized) environmentally-induced rotations about a different axis. In addition to this primary objective, there are other (potentially competing) constraints and targets, such as (a) minimizing the total time required to perform operations relative to decoherence time scales, (b) minimizing the control

field fluence/intensity, (c) designing controls based on electronics/physical constraints, and (d) locating controls that are robust to control and/or system uncertainties.

This article is organized as follows. Section II introduces and develops the model qubit system that we use for our optimizations and simulations. This system is physically motivated by a double quantum dot (DQD) semiconductor qubit. A system of natural units is defined that allows us to compare our results to relevant experimental parameters. In section III, we summarize our gradient-based OC routine, describing our control objective and numerical procedure. Section IV presents OC results for subsequent comparison to those from the DD+OC QCP. Inherent robustness of these OCs is also analyzed. Section V summarizes the control-field criteria developed by Pasini *et al.* for designing control pulses that are robust to decoherence [7]. Our adaptation of these criteria to closed-system unitary control is also described and the DD+OC control problem is presented. In section VI, we qualitatively explain and mathematically formulate our method for solving this nonlinearly-constrained control problem. Section VII presents results from our DD+OC optimization algorithm. Fidelity and robustness of the control fields are numerically analyzed and discussed. We also compare OC and DD+OC results to illustrate the benefit of our hybrid approach. We conclude this article in section VIII with a brief summary of our results and identify several future directions of our research.

II. LANDAU-ZENER MODEL SYSTEM

A. Model Hamiltonian

We represent the dynamical model of a qubit with the following effective Hamiltonian ($\hbar \equiv 1$) [11]:

$$H(t) := \varepsilon S_x + C(t)S_z, \quad (1)$$

where $S_\lambda = \sigma_\lambda/2$ is a spin operator for an effective spin-1/2 particle, σ_λ is a Pauli matrix ($\lambda \in \{x, y, z\}$), $C(t)$ represents the time-dependent control field, and εS_x characterizes a persistent (and potentially time-dependent) rotation about the x -axis. Note that $H(t)$ corresponds to the two-state Landau-Zener model [9]. Note that both $C(t)/\hbar$ and ε/\hbar have units of angular frequency, e.g., radians per second in SI units.

Let \mathcal{H} denote the Hilbert space of the system, where $n := \dim\{\mathcal{H}\} = 2$, and $\{|S_i\rangle\}$

denote the orthonormal basis of S_z that spans \mathcal{H} that we designate as the computational basis. The group of all unitary operators on \mathcal{H} is denoted by $U(\mathcal{H})$. In general, the unitary time-evolution operator $U(t) \in U(\mathcal{H})$ for a closed quantum system obeys the time-dependent Schrödinger equation ($\hbar \equiv 1$):

$$\dot{U}(t) = -iH(t)U(t), \quad (2)$$

where $U(t=0) = \mathbb{1}_n$, the $n \times n$ identity matrix. From a controllability perspective [12, 13], the Hamiltonian in Eq. (1) generates the Lie algebra $\mathfrak{su}(2)$. Thus, the system is completely dynamically controllable, i.e., any element of the Lie group $SU(2)$ can be generated via Eq. (2). However, this analysis does not necessarily reveal anything about the control-field structure necessary to realize an arbitrary $SU(2)$ operation. As an illustrative example of our DD+OC QCP, we focus on constructing unitary operations corresponding to $\pi/2$ - and π -rotations about the z -axis.

B. Double quantum dot logical qubit

Although our qubit model is quite general, we refer to a particular application of a DQD solid-state qubit [14, 15], which has been studied in an array of experiments, e.g., [11, 16–19]. With one electron in each quantum dot, the DQD system spans four spin states. An applied magnetic field will break the degeneracy of the states in which both electrons are either aligned with or against the field. In this situation, it is possible (and often advantageous) to work within the two-level subspace where the net spin angular momentum is zero. By adjusting voltages in the electrostatically defined quantum dots, the magnitude of the exchange interaction, J , between the electrons may be controlled. This interaction controls the splitting between the singlet, $|S\rangle = (|\uparrow\downarrow\rangle - |\downarrow\uparrow\rangle)/\sqrt{2}$ and triplet, $|T_0\rangle = (|\uparrow\downarrow\rangle + |\downarrow\uparrow\rangle)/\sqrt{2}$, states of the spin-zero manifold. Designating $|\mathcal{S}_0\rangle = |S\rangle$ and $|\mathcal{S}_1\rangle = |T_0\rangle$, we equate $C(t)$ in our general model [Eq. 1] with J .

The spin-zero manifold is insensitive to a global magnetic field. However, gradients in the magnetic field will cause singlet-triplet transitions. Such a gradient splits the energy of the states $|\uparrow\downarrow\rangle = (|T_0\rangle + |S\rangle)/\sqrt{2}$ and $|\downarrow\uparrow\rangle = (|T_0\rangle - |S\rangle)/\sqrt{2}$ by the difference in effective Zeeman energies for an electron in either of the two quantum dots. We may therefore equate ε with this effective Zeeman energy difference. In GaAs DQD systems, the effective Zeeman energy difference is typically dominated by the Overhauser shifts from a lattice of

randomly polarized nuclear spins corresponding to approximately 0.1-1 μeV [15]. It has been demonstrated that a desired difference in Overhauser shift of a GaAs DQD may be realized through feedback control from a preparatory qubit [19]. However, the value of ε will drift over time through the nuclear spin diffusion that causes spectral diffusion [2, 20–22], motivating the need for robust control. In proposed Si DQD systems, e.g., Ref. [23], nuclear spins may be eliminated through isotopic enrichment. Other spin baths, such as electron spins of donor impurities [24] or dangling bond spins at an interface [25], may also lead to variations and drift in ε .

C. Natural units

In addition to setting $\hbar \equiv 1$ (corresponding to unit of angular momentum: energy \times time), a simple set of natural units is defined by also setting the final time $t_f \equiv 1$. The ratio $\hbar/t_f = 1$ yields the natural unit of energy, which, when $t_f = 20$ ns (as an example), corresponds to approximately 5.273×10^{-27} J or 3.291×10^{-8} eV. By appropriately scaling the Hamiltonian and control field, this propagation time can be transformed to any t_f . Relationships between these natural units and SI units are summarized in Table I.

In this work, optimizations were performed for individual values of $\varepsilon \in [0, 5.0]$; we denote the nominal values of ε used in these simulations as ε_0 . This range of ε corresponds to no and moderate rotations from the environment for the DQD example. For a DQD logical qubit,

$$\varepsilon = g_e \mu_B B_\Delta / \hbar, \quad (3)$$

where g_e is the so-called electron g-factor, μ_B is the Bohr magneton, B_Δ is the magnetic field resulting from the difference in the random hyperfine fields from each quantum dot along the direction of the applied field, and \hbar is the reduced Planck constant. When 1 natural unit of time equals 20 ns (a decent estimate of the time required for one-qubit rotations for a DQD system [11]), $\varepsilon = 5.0$ natural units of angular frequency (the maximum value of ε_0 considered) corresponds to $B_\Delta \approx 6.5$ mT; this is reasonably consistent with experimental reports of GaAs DQDs [11, 14, 15].

Quantity	Natural unit	SI unit
\hbar	angular momentum	1.055×10^{-34} J s
t	time	20.0×10^{-9} s
C	energy	5.273×10^{-27} J

TABLE I: Natural and SI units for the logical qubit described by the Hamiltonian in Eq. (1).

III. OPTIMAL CONTROL OF UNITARY OPERATIONS VIA GRADIENT-BASED ALGORITHMS

A. Objective functionals for unitary operations

For a target unitary operation $V \in U(\mathcal{H})$, the distance Δ between V and a simulated final-time unitary U_{t_f} is calculated as

$$\Delta[V, U(t_f)] := \sqrt{1 - \frac{1}{n} |\text{Tr}[V^\dagger U(t_f)]|}. \quad (4)$$

This phase-invariant distance measure is a special case of a more general distance measure developed in Ref. [26], which is applicable to studies involving composite systems where only the system/qubit dynamics are directly of interest [27]. For the purpose of this work, the terms “distance” and “error” are synonymous.

Concerning mathematical notation, because the unitary time-evolution operator is a function of time and a functional of the control, it will be expressed more generally as $U(t; C)$ for all time t and a given control C , compared to $U(t)$; the final-time unitary operation will be expressed more generally as $U_{t_f}(C)$, compared to $U(t_f)$. Also, we denote the space of such controls with final time $t = t_f$ as \mathfrak{C}_{t_f} . Properties of the Hilbert space \mathfrak{C}_{t_f} are discussed in Ref. [26] and the following sections.

Because $0 \leq \Delta \leq 1$ in general, it is convenient to define the fidelity \mathcal{F} of unitary operations as [26, 28]

$$\mathcal{F} := \frac{1}{n} |\text{Tr}[V^\dagger U(t_f)]| = 1 - \Delta^2(V, U_{t_f}), \quad (5)$$

which is a common measure of gate fidelity based on the Hilbert-Schmidt inner product [29, 30]. Note the quadratic dependence of \mathcal{F} on Δ , e.g., a distance of 10^{-6} corresponds to a fidelity of $1 - 10^{-12}$.

An optimal control (OC) field for unitary operations is located by minimizing an objective functional $\mathcal{J}[C]$ that incorporates the final-time unitary target V , constrains the dynamics of $U(t)$ to evolve according to Eq. (2), and penalizes the fluence of the control field. For this work, the objective functional is defined as:

$$\mathcal{J}[C] := \Delta[V, U_{t_f}(C)] + \frac{\alpha}{2} \int_0^{t_f} \frac{C^2(t)}{s(t)} dt. \quad (6)$$

The optimization is performed using a gradient-based algorithm (GrA; see [26, 27, 29, 31] for details and examples of gradient-based optimization). Here, $s : [0, t_f] \rightarrow \mathbb{R}$ is a continuous and non-negative ‘‘shape function’’ and $\alpha \geq 0$ weights the cost of the control field fluence relative to the distance Δ . When appropriately chosen, $s(t)$ can move undesirably-shaped functions so they are less likely to be optimization targets [26]. In this work, we use $s(t) = \sin^{1/p}(\pi t/t_f)$, where $p \in \mathbb{Z}_+$. This form constrains the control-field slew rate for the initial and final times.

For the time-dependent Hamiltonian in Eq. (1), $U_{t_f} : \mathfrak{C}_{t_f} \rightarrow U(\mathcal{H})$ denotes the map, defined implicitly through the Schrödinger equation [Eq. (2)], that takes a control field $C(t) \in \mathfrak{C}_{t_f}$ to the unitary time-evolution operator $U_{t_f} \in U(\mathcal{H})$. Note that \mathfrak{C}_{t_f} is a Hilbert space of admissible controls, on which $U(t; C)$ exists for all $t \in [0, t_f]$ and all $C \in \mathfrak{C}_{t_f}$ [32], where the inner product on \mathfrak{C}_{t_f} is

$$\langle f, g \rangle_{\mathfrak{C}_{t_f}} := \int_0^{t_f} \frac{f(t)g(t)}{s(t)} dt, \quad \forall f, g \in \mathfrak{C}_{t_f}. \quad (7)$$

As such, $\mathcal{J} : \mathfrak{C}_{t_f} \rightarrow \mathbb{R}$ is the *dynamical* version of the distance measure Δ , with a relative cost on the control field fluence, determined by α .

B. Optimization with a gradient-based algorithms

This section briefly summarizes the variational analysis of \mathcal{J} and describes criteria for the optimal points (or submanifolds) of \mathcal{J} with respect to $C(t)$. The gradient of the objective functional \mathcal{J} is explicitly derived in Ref. [26], we present it here for continuity:

$$(\nabla \mathcal{J}[C])(t) = \frac{s(t)}{4n \Delta[V, U_{t_f}(C)]} \text{Im} \left(\text{Tr} \left\{ [U_{t_f}^\dagger(C)R - R^\dagger U_{t_f}(C)] U^\dagger(t; C) S_z U(t; C) \right\} \right) + \alpha C(t), \quad (8)$$

where $R = \exp(-i\phi)V$, $\phi = \text{Im} \{ \ln [\text{Tr} (V^\dagger U_{t_f})] \}$. Critical points of \mathcal{J} are defined as controls for which $(\nabla \mathcal{J}[C])(t) = 0$ for any time t [33].

Given the k th iterate of the control field $C^{(k)}(t)$, adjustments to the control field for the $(k+1)$ th iteration are given by

$$C^{(k+1)}(t) := C^{(k)}(t) - \beta (\nabla \mathcal{J} [C^{(k)}]) (t), \quad (9)$$

where β is a constant that determines the magnitude of the field adjustment. This procedure describes an implementation of a steepest descent algorithm [34]. Initial control fields $C^{(0)}(t)$ have the parameterized form

$$C^{(0)}(t) := f(t) \sum_i a_i \cos(\omega_i t + \delta_i), \quad (10)$$

where $f(t)$ is an envelope function (e.g., a Gaussian) that incorporates control field duration and width, and a_i , ω_i , and δ_i are the amplitude, frequency, and relative phase of the i th control field component. The frequencies ω_i may be determined from the system Hamiltonian. Parameterized controls, such as those described by Eq. (10), are often used in hybrid optimization schemes combining evolutionary and gradient-based optimization algorithms, e.g., [27, 35].

IV. RESULTS FROM QUANTUM OPTIMAL CONTROL

Using the GrA discussed in section III, OCs were found for unitary targets that perform $\pi/2$ - and π -rotations about the z -axis:

$$Z_\theta := \begin{pmatrix} \exp(-i\theta/2) & 0 \\ 0 & \exp(i\theta/2) \end{pmatrix}, \quad (11)$$

where $\theta \in \{\pi/2, \pi\}$. The final time for all OCs was fixed at $t_f = 1$ natural unit of time. Optimizations were performed individually for *specific* angular frequencies: $\varepsilon_0 \in [0, 5]$. As described in section II C, this interval represents the regime of no to moderate rotations from the environment for the DQD logical qubit. To emphasize the ε -specific nature of these OCs, we denote them as $C_o(\varepsilon_0; t)$.

Because of the similarity of results over the entire interval $0 \leq \varepsilon \leq 5$, only a subset will be presented. OC fields for $Z_{\pi/2}$ and Z_π as a function of ε are presented in Figs. 1 and 2, respectively. Although all of these OCs were located using the same initial control field, which is very similar to the OC reported for $\varepsilon_0 = 0$, the converged fields differ dramatically

for different values of ε . All OCs have distances $\Delta < 10^{-6}$ (or $\mathcal{F} > 1 - 10^{-12}$, basically corresponding to the limits of numerical precision), which is expected because this system is relatively simple and fully controllable [12, 13]. For $\varepsilon_0 = 0$, all OCs for Z_θ satisfy

$$\theta(t_f; C) = \int_0^{t_f} C(t)dt + 2m\pi, \quad (12)$$

for some $m \in \mathbb{Z}$, i.e., OC design simple corresponds to pulse-area control in this situation. However, when $\varepsilon \neq 0$, there is no corresponding pulse-area requirement. In fact, if ε is known accurately, it is possible to perform Z_θ operations with piecewise constant controls that integrate to zero. Table II contains information about some of the properties of these OCs. For the DQD qubit, we observe that these controls require negative exchange coupling values. Although negative exchange energy is uncommon, it is predicted to be possible to produce through combined tuning of the magnetic field, dot size, and tunnel coupling [36].

Target operation: $Z_{\pi/2}$

ε_0	0	1	2	3	4	5
$\max C_o(\varepsilon_0; t) $	2.4	18.5	18.4	18.3	6.7	5.9
θ	$\pi/2$	1.5779	1.600	1.640	-3.433	-2.566
\mathcal{E}	3.4	84.5	83.0	18.3	6.7	5.9
$\Delta(Z_{\pi/2}, U_{t_f})$	1.86×10^{-7}	9.15×10^{-7}	4.94×10^{-8}	1.39×10^{-7}	3.13×10^{-8}	4.30×10^{-8}

Target operation: Z_π

ε_0	0	1	2	3	4	5
$\max C_o(\varepsilon_0; t) $	4.8	12.2	12.1	11.9	11.6	11.4
θ	π	3.1020	2.9824	2.7802	2.4923	2.1181
\mathcal{E}	13.7	39.5	38.4	36.5	34.1	31.4
$\Delta(Z_\pi, U_{t_f})$	7.96×10^{-8}	6.51×10^{-7}	4.21×10^{-8}	1.67×10^{-7}	1.63×10^{-7}	2.37×10^{-7}

TABLE II: Performance of the OCs for one-qubit Z_θ operations. Here, $\max |C_o(\varepsilon_0; t)|$, θ , $\mathcal{E} = \int_0^{t_f} C_o^2(\varepsilon_0; t)dt$, and $\Delta(Z_\theta, U_{t_f})$ are the maximum control field amplitude, angle of controlled z -axis rotation, control field fluence, and gate distance, respectively, in the corresponding natural units described in section II C.

Interestingly, for both $Z_{\pi/2}$ and Z_π operations, although both OCs $C_o(1; t)$ and $C_o(2; t)$ have very similar structures, their distance responses to variations in ε are quite different,

as shown in Figs. 3 and 4, respectively. Even with $\max_t |C_o(1;t) - C_o(2;t)| < 0.2$ (see inset of Figs. 1 and 2), it is interesting to note that this two-level system behaves like an effective control-field spectrometer. The sensitivity of this system to relatively small control field variations combined with the inherent noise present in most controls warrants further study of the impact that realistic control field fluctuations may have on practical fault-tolerant QC [30, 37].

Quantum computing architectures often assume encoded quantum operations to correct the inevitable errors due to control and environmental noise. Gate operations, such as Z_θ simulated here, must achieve a minimum fidelity threshold for successful quantum error correction. The predicted maximum error of less than 10^{-6} for $\varepsilon \in [0, 5]$ is within typical ranges necessary for fault-tolerant QC [1, 15, 23]. These results highlight the potential advantage of using OC if estimates of Hamiltonian parameters are known well. However, OCs are not necessarily robust to uncertainty in the magnitude of the environmental rotation ε . Uncertainty can result from incomplete or poor system parameter estimates as well as from dynamics of the environment [20, 24].

To investigate inherent robustness with respect to variations in ε quantitatively, control fields optimized for a particular values of ε [i.e., $C_o(\varepsilon_0;t)$] were subsequently applied to a surrounding interval of ε ; results are presented in Fig. 3 and 4, for the $Z_{\pi/2}$ and Z_π operations, respectively. Consider the distance response of $C_o(2;t)$ to variations in ε , which varies substantially with respect to variations that correspond to ~ 1 mT fluctuations for DQD systems. Without specifying a measure of robustness as an additional control objective, the resulting OCs are not inherently robust to modest local magnetic-field fluctuations (e.g., at each quantum dot). This indicates that error in measurement fidelity used to characterize ε must be approximately 10^{-6} or smaller to realize gates with errors that are approximately 10^{-6} . Moreover, with these controls, ε could not drift during a computation without serious fidelity loss.

V. ROBUST DYNAMICAL DECOUPLING PULSES

Optimization of the functional \mathcal{J} in Eq. (6) is highly under-determined and multiple control fields exist that will produce the same target operator V [38, 39]. Requiring robustness to control and/or system variations involves the specification of additional constraints

or penalties, thereby limiting solutions to this OC problem. In this section, we summarize a set of control constraints that characterize control robustness for decoherence and adapt them to locate controls that are robust to system noise.

A. General robustness criteria

Consider the following open-system Hamiltonian for one qubit:

$$H_{\text{open}} = \vec{S} \cdot \vec{C}(t) + \vec{S} \cdot \vec{\Gamma} + H_e, \quad (13)$$

where $\vec{S} = (S_x, S_y, S_z)$ represents the spin-operator vector, $\vec{C}(t) = (C_x, C_y, C_z)$ represents a multi-polarized control field, $\vec{\Gamma} = (\Gamma_x, \Gamma_y, \Gamma_z)$ represents the environment interaction operator, and H_e represents the environment Hamiltonian. By analyzing the resulting unitary time-evolution operator generated by H_{open} , Pasini *et al.* have identified control-field criteria necessary to eliminate first- and second-order effects resulting from the environment Hamiltonian H_e and the interaction term $\vec{S} \cdot \vec{\Gamma}$ [7]. Although applicable to multi-polarized controls and general qubit-environment coupling, the methodology developed in this section assumes control-qubit coupling along the z -axis and qubit-environment interaction along the x -axis, i.e.,

$$H'_{\text{open}} = C(t)S_z \otimes \mathbb{1}_{n_e} + S_x \otimes \Gamma_x + \mathbb{1}_2 \otimes H_e, \quad (14)$$

where \mathcal{H}_e is the Hilbert space of the environment and $n_e := \dim\{\mathcal{H}_e\}$. For controlled $\pi/2$ - and π rotations about the z -axis, Pasini *et al.* derived the following vector expression to constrain the space of controls to suppress errors resulting from an x -axis environment interaction:

$$\vec{\zeta}[\theta] := (\zeta_1, \zeta_2, \zeta_3, \zeta_4, \zeta_5)^T, \quad (15a)$$

where

$$\zeta_1[\theta] := \int_0^{t_f} \sin[\theta(t)] dt, \quad (15b)$$

$$\zeta_2[\theta] := \int_0^{t_f} \cos[\theta(t)] dt, \quad (15c)$$

$$\zeta_3[\theta] := \int_0^{t_f} \int_0^{t_f} \sin[\theta(t_1) - \theta(t_2)] \text{sgn}(t_1 - t_2) dt_1 dt_2, \quad (15d)$$

$$\zeta_4[\theta] := \int_0^{t_f} t \sin[\theta(t)] dt, \quad (15e)$$

$$\zeta_5[\theta] := \int_0^{t_f} t \cos[\theta(t)] dt, \quad (15f)$$

and

$$\theta(t; C) := \int_0^t C(\tau) d\tau. \quad (16a)$$

The angle θ corresponds to the rotation performed by the control field during the time interval $[0, t]$. Although θ is a functional of the control field $C(t)$, whenever appropriate we abbreviate $\theta(t; C)$ as $\theta(t)$ to avoid unnecessarily cumbersome notation. Equation (16a) is equivalent to

$$\frac{d\theta(t; C)}{dt} = C(t). \quad (16b)$$

Also,

$$\frac{\delta\theta[t; C]}{\delta C(t')} = \mathfrak{H}(t - t'), \quad (16c)$$

where $\mathfrak{H}(t - t')$ is the Heaviside step function:

$$\mathfrak{H}(t' - t) := \begin{cases} 1 & \text{when } t \geq t' \\ 0 & \text{when } t < t' \end{cases} \quad (17)$$

For convenience and simplicity in the analysis that follows this section, we define $\vec{\eta}$ as

$$\vec{\eta}[C] := (\eta_1, \eta_2, \eta_3, \eta_4, \eta_5)^T, \quad (18a)$$

where

$$\eta_i := \zeta_i \circ \theta. \quad (18b)$$

Thus, $\vec{\eta} : \mathfrak{C}_{t_f} \mapsto \mathbb{R}^5$. For one qubit, the components of $\vec{\eta}$ represent the first- and second-order errors, with respect to the final time t_f and error Hamiltonian, of a controlled $\pi/2$ -

or π -rotation about the z -axis. Specifically, η_1 and η_2 represent first-order errors, while η_3 , η_4 , and η_5 represent second-order errors. Thus, when $\vec{\eta} \equiv 0$, the pulse is accurate up to third-order, eliminating first- and second-order effects resulting from the interaction of the qubit with the environment. According to the analysis in Ref. [7], when $[H_e, \Gamma_\lambda] = 0$, for all λ , components η_4 and η_5 can be neglected from the vector constraint [Eq. (18)].

B. Closed-system robustness criteria

To apply these results to a closed one-qubit system and construct robust Z_θ operations for the DQD logical qubit using this criteria, we first compare the Hamiltonians H in Eq. (1) and H'_{open} in Eq. (14). These Hamiltonians are equal if $\Gamma_x = \varepsilon$ and $H_e = 0$, which implies that $[H_e, \Gamma_\lambda] = 0$, so $\vec{\eta}^r := (\eta_1, \eta_2, \eta_3)^T$ is the relevant *reduced* vector constraint. Incorporating these nonlinear equality constraints into the original optimization problem yields the following nonlinearly-constrained control problem:

$$\begin{aligned} & \min_{C \in \mathcal{C}_{t_f}} \mathcal{J}[C] \\ & \text{subject to} \\ & \vec{\eta}^r[C] = 0, \end{aligned} \tag{19}$$

Methods such as diffeomorphic modulation under observable-response-preserving homotopy (DMORPH) [30, 40] or sequential quadratic programming [41] are necessary to generate OCs that maintain or satisfy approximate feasibility, determined by $\vec{\eta}^r = 0$. A technique using DMORPH is developed in the next section.

For a DQD qubit described by the Hamiltonian in Eq. (1), control fields and corresponding distances for $\pi/2$ - and π -pulses from Ref. [7] satisfying $\vec{\eta}^r = 0$ are presented in Figs. 5 and 6, respectively. These fields are denoted as $C_d(t)$. Incorporating the control-field constraints specified by Pasini *et al.* [7], first- and second-order errors can be eliminated. As such, gate distance increases with the magnitude of ε and optimum performance occurs when $\varepsilon = 0$, which is not necessarily expected to be valid for actual DQD experiments, e.g., [11].

VI. HYBRID QUANTUM CONTROL: DYNAMICAL DECOUPLING + OPTIMAL CONTROL

Given the favorable structure of quantum control landscapes, e.g., trap-free structure, connected submanifolds corresponding to optimal solutions, etc. [37–39], DMORPH provides a mathematical means to explore families of controls that achieve the same objective [30, 40]. Applications of DMORPH include the continuous variation of a Hamiltonian while preserving the value of a quantum-mechanical observable [40] and exploring the level sets of state and unitary control [30, 40, 42]. DMORPH can also be used as direct optimization technique. In this work, we use DMORPH techniques to explore the space of controls corresponding to $\vec{\eta} = 0$ while optimizing \mathcal{J} for a specified ε_0 .

In this section we develop a method to optimize \mathcal{J} over the set $\mathfrak{C}_{t_f}^\eta := \vec{\eta}^{-1}(0) \subset \mathfrak{C}_{t_f}$, the preimage of $\vec{\eta}$, i.e., the region of feasible controls satisfying $\vec{\eta} = 0$. To increase general applicability, we develop this technique for $\vec{\eta}$, rather than only $\vec{\eta}^r$. Away from critical points of $\vec{\eta}$, $\mathfrak{C}_{t_f}^\eta$ is a codimension 5 submanifold of \mathfrak{C}_{t_f} [43]. It is assumed that critical points of $\vec{\eta}$ are rare, an assumption supported by the success of the resulting algorithm. Then, the gradient of the restricted function $\mathcal{J}|_{\mathfrak{C}_{t_f}^\eta}$ at a point $C \in \mathfrak{C}_{t_f}^\eta$ is just the projection of the gradient of \mathcal{J} at C onto the tangent space $T_C \mathfrak{C}_{t_f}^\eta$ of $\mathfrak{C}_{t_f}^\eta$ at C [30, 44, 45]. By systematically updating the control field iteratively using a GrA with this projected gradient, the algorithm is able to simultaneously improve the value of \mathcal{J} and maintain approximate feasibility, or at least impede deviations from feasibility.

A. Gradient of the feasibility space

Using DMORPH to remove the components of $\nabla \mathcal{J}[C]$ that cause a change in $\vec{\eta}$ requires the gradient of each element of $\vec{\eta}$, $\nabla \eta_i[C]$:

$$\nabla \eta_i[C] = \int_0^{t_f} \frac{\delta \zeta_i[\theta]}{\delta \theta(\tau)} \times \frac{\delta \theta(\tau)}{\delta C(t)} d\tau = \int_t^{t_f} \frac{\delta \zeta_i[\theta]}{\delta \theta(\tau)} d\tau \Rightarrow \quad (20a)$$

$$\begin{pmatrix} \nabla \eta_1[C] \\ \vdots \\ \nabla \eta_5[C] \end{pmatrix} = \begin{pmatrix} \int_t^{t_f} \cos[\theta(\tau)] d\tau \\ \int_t^{t_f} \sin[\theta(\tau)] d\tau \\ 2 \int_t^{t_f} \int_0^{t_f} \{ \cos[\theta(\tau)] \cos[\theta(\tau')] + \sin[\theta(\tau)] \sin[\theta(\tau')] \} \text{sgn}(\tau - \tau') d\tau' d\tau \\ \int_t^{t_f} \tau \cos[\theta(\tau)] d\tau \\ \int_t^{t_f} \tau \sin[\theta(\tau)] d\tau \end{pmatrix}. \quad (20b)$$

As expressed here, the vector of η_i -gradients is a function of the time variable t .

B. Gradient projection method

In addition to the gradients $\nabla \eta_i[C]$, we also need a vector that specifies the relative direction or weight of each gradient component that we want to remove. This is determined by first calculating the Gramian matrix, with elements

$$(G_c)_{ij} := \langle \nabla \eta_i[C], \nabla \eta_j[C] \rangle_{\mathbf{e}_{t_f}}. \quad (21)$$

In general, G_c is not guaranteed to be full rank. Non-singularity of G_c must be explored (numerically) as a function of C . However, if $\nabla \eta_i$ are all linearly independent, then G_c is invertible. With Eqs. (20) and (21), all gradient directions of $\nabla \eta_i$ can be removed from $\nabla \mathcal{J}$ as follows:

$$\nabla \mathcal{K}[C] := \nabla \mathcal{J}[C] - \sum_{i=1}^5 \nabla \eta_i[C] \{ G_c^{-1} [\vec{q}_c (\nabla \mathcal{J}[C])] \}_i, \quad (22a)$$

where \vec{q}_c is

$$[\vec{q}_c (\nabla \mathcal{J}[C])]_i := \langle \nabla \mathcal{J}[C], \nabla \eta_i[C] \rangle_{\mathbf{e}_{t_f}}. \quad (22b)$$

Thus, $\nabla \mathcal{K}$, is an element of the tangent space $T_C \mathcal{J}$ of \mathcal{J} at C that decreases \mathcal{J} without changing the value of η , provided the multiplier β in Eq. (9) is selected properly, i.e., β is

within the validity of the linear approximation of the tangent space at C . Eq. (22a) projects $\nabla\mathcal{J}[C]$ onto $T_C\mathfrak{C}_{t_f}^\eta$, rather than just $T_C\mathfrak{C}_{t_f}$. That $\nabla\mathcal{K}[C]$ is orthogonal to $\nabla\eta_i[C]$ for all i can be verified as follows. For example, let

$$\xi := \sum_{i=1}^5 \chi_i \nabla\eta_i[C], \quad (23)$$

i.e., ξ is a linear combination of $\{\nabla\eta_i[C]\}$, where $\chi_i \in \mathbb{R}$. Replacing $\nabla\mathcal{J}[C]$ with ξ in Eq. (22a) yields

$$\xi - \sum_{i=1}^5 \nabla\eta_i[C] \{G_c^{-1}[\vec{q}_c(\xi)]\}_i = \xi - \sum_{i=1}^5 \nabla\eta_i[C] (G_c^{-1}G_c\vec{\chi})_i = 0, \quad (24)$$

where $\vec{\chi} := (\chi_1, \chi_2, \chi_3, \chi_4, \chi_5)^T$.

As mentioned in the introduction, because we combine methods from DD and OC to generate improved control fields, we denote the integrated optimization procedure described in this section as DD+OC. Straightforward modifications of G_c and \vec{q}_c are required when $\vec{\eta}^r$ is the constraint vector rather than $\vec{\eta}$, i.e., $G_c \in \mathcal{M}_3(\mathbb{R})$, rather than $\mathcal{M}_5(\mathbb{R})$, and $\vec{q}_c(\nabla\mathcal{J}[C]) \in \mathbb{R}^3$, rather than \mathbb{R}^5 .

VII. RESULTS FROM DYNAMICAL DECOUPLING + OPTIMAL CONTROL

Using the DD+OC procedure described in section VI, we seek to numerically explore the space of controls for those satisfying $\vec{\eta}^r = 0$ and $\Delta = 0$ to improve control fidelity for $Z_{\pi/2}$ and Z_π operations. To a certain extent, the minimization of Δ and $\vec{\eta}$ are competing control objectives. Compare the OC distance plots (Figs. 3 and 4) to those for DD (Fig. 6). OC for the design of unitary operations, as we have formulated it, seeks to minimize Δ for a particular value of ε . Because the system [Eq. (1)] is controllable and the underlying control landscape possesses a fortuitous trap-free topological structure [38, 39], a GrA achieves this objective quite successfully. However, these OCs are not robust to perturbations in ε , whereas controls satisfying $\vec{\eta}^r = 0$ are optimal for $\varepsilon_0 = 0$ and near-optimal for ε_0 near zero. This scenario illustrates the balance between fidelity and robustness. Overall, the DD pulses are reasonably robust to perturbations in ε , provided that ε and/or $\Delta\varepsilon$ are not too large. Given that these two control objectives are potentially competing, we use the hybrid optimization procedure developed in section VI to suppress deviations from $\vec{\eta}^r = 0$, but not

entirely eliminate them. In other words, convergence of the DMORPH DD+OC algorithm occurs only when \mathcal{J} stops decreasing.

Because the formulation of OC requires the specification of ε , we consider $\varepsilon_0 \in [0, 5.0]$. Results for the $Z_{\pi/2}$ and Z_π operations are quite similar, so we focus our discussion on the results for Z_π . The final time for all DD+OCs was fixed at $t_f = 1$ natural unit of time. DD+OC fields for Z_π are presented in Fig. 7. These fields are denoted as $C_h(\varepsilon_0; t)$ where the subscript ‘‘h’’ indicates the hybrid feature of our approach. Corresponding results for gate distance Δ and $|\vec{\eta}^r|$ are presented in Figs. 8 and 9, respectively. We note that the converged results deviate substantially from $\vec{\eta} \approx 0$ in some cases. In addition, table III contains information about some of the properties of these DD+OC fields. The converged DD+OC fields for $\varepsilon_0 \in \{0, 1, 2, 3, 4\}$ are very similar, supporting the observation in section IV that this system behaves like an effective spectrometer. Interestingly, the DD+OC field for $\varepsilon_0 = 5.0$ has rather unique features compared to the fields for other values of ε . Based on distance response of the corresponding $C_d(t)$ control, this value of ε_0 is not within the perturbative limit of the analysis that produced the vector constraint $\vec{\eta}$. With such a large distance at $\varepsilon_0 = 5.0$, the DD+OC routine improves the distance by approximately three orders of magnitude and simultaneously improves the robustness for $4.5 \leq \varepsilon \leq 5.5$. Figure 8 compares the distance of $C_d(t)$ and $C_h(\varepsilon_0; t)$ control fields. All control fields $C_h(\varepsilon_0; t)$ exhibit improved robustness to ε -perturbations in a neighborhood around the nominal value ε_0 used in the DD+OC algorithm. This result demonstrates the utility of combining so-called ‘‘pre-design’’ methods, such as the DD pulses by Pasini *et al.* [7], with OC and estimates of system parameters. By combining these QCPs, we have developed a form of hybrid quantum control; estimates of system parameters can be directly incorporated into simulations to generate improved quantum operations for information processing and memory.

Figure 9 compares distance Δ and $|\vec{\eta}^r|$ as a function of the optimization iteration. For the most part, $|\vec{\eta}^r|$ increases as Δ decreases, which is consistent with competing control objectives. Although components of $\nabla\mathcal{J}$ that are parallel to all gradients $\nabla\eta_i$ are removed, $\vec{\eta}$ increases during the optimization for two reasons: (a) Eq. (22a) removes components of $\nabla\eta_i$ (where elements η_i are *nonlinear* functions of the control) using an iterative linear projection method and (b) convergence of the DD+OC routine does not depend on $|\vec{\eta}|$.

To collectively compare results from DD, OC, and DD+OC, Z_π gate distance data from Fig. 4 and 8 are presented together in Fig. 10. Although the OC fields $C_o(\varepsilon_0; t)$ often

outperform the DD+OC fields $C_h(\varepsilon_0; t)$, the OCs $C_o(\varepsilon_0; t)$ do not have the robustness of the DD+OC fields $C_h(\varepsilon_0; t)$. To emphasize this feature, Figures 11 and 12 present Z_π gate distances for $C_o(\varepsilon_0; t)$, $C_d(t)$, and $C_h(\varepsilon_0; t)$ controls in an interval centered at $\varepsilon_0 = 1$ and $\varepsilon_0 = 2$, respectively. $C_o(1; t)$ is very sensitive to variations in ε ; when ε changes from 1 to 1 ± 0.02 (a change corresponding to approximately 2.6×10^{-5} mT), the gate distance increases substantially from 10^{-6} to 10^{-3} . Similarly, for $C_o(2; t)$, when ε changes from 2 to 2 ± 0.02 , the gate distance increases from 10^{-7} to 10^{-3} . However, for $C_h(\varepsilon_0; t)$, as ε varies from ε_0 , the increase in gate distance is much more gradual.

Target operation: $Z_{\pi/2}$

ε_0	0	1	2	3	4	5
$\max C $	29.5	29.5	29.3	29.2	29.4	29.6
θ	$\pi/2$	$\pi/2$	1.5704	1.5691	1.5697	1.5792
\mathcal{E}	335.5	334.7	332.9	337.5	356.5	370.6
$\Delta(Z_{\pi/2}, U_{t_f})$	1.69×10^{-7}	2.71×10^{-5}	3.34×10^{-5}	3.78×10^{-5}	7.68×10^{-5}	2.91×10^{-5}

Target operation: Z_π

ε_0	0	1	2	3	4	5
$\max C $	28.8	28.8	28.7	28.4	28.2	28.7
θ	π	π	3.1411	3.1391	3.1357	3.137
\mathcal{E}	264.8	264.0	261.8	259.1	259.25	273.7
$\Delta(Z_\pi, U_{t_f})$	1.21×10^{-7}	1.11×10^{-5}	2.56×10^{-5}	1.46×10^{-5}	1.59×10^{-5}	9.69×10^{-6}

TABLE III: Performance of the DD+OC for one-qubit Z_θ operations. Here, $\max(C)$, θ , $\mathcal{E} = \int_0^{t_f} C^2(t)dt$, and $\Delta(Z_\theta, U_{t_f})$ are the maximum control field amplitude, angle of controlled z -axis rotation [as defined in Eq. (16a)], control field fluence, and gate distance, respectively, in the natural units described in section II C.

VIII. CONCLUSIONS AND FUTURE DIRECTIONS

Combining OC with the robustness criteria established by Pasini *et al.* introduces improvements to the control of quantum systems for information processing. Given a good characterization of the magnitude ε of a persistent, but somewhat uncertain rotation about

the x -axis, a near-optimum fidelity can be achieved for $\varepsilon > 0$. Furthermore, the DD+OC fidelity exhibits improved robustness to uncertainty in ε , compared to the original DD pulses. The systematic integration of DD and OC, therefore, promises considerable improvement over DD or OC strategies alone. We have provided a quantitative illustration for a logical qubit based on a DQD system, with continuous controls that possess reasonable magnitudes [36], based on the natural-to-SI unit mapping.

We are currently investigating the benefits of these DD+OC $\pi/2$ - and π -pulses for memory and information processing in the presence of a decohering spin bath. It will be useful to determine how these pulses extend spin-echoes and improve more general DD sequences, such as those described in Refs. [2, 5, 46]. Future work involves an exploration of unitary control sensitivity to fluctuations in the control field itself (e.g., control noise). Both OC and DD+OC results suggest that these fluctuations may contribute just as significantly to gate errors as system/environment fluctuations. Robust solutions are crucial for practical fault-tolerant QC. Extensions of the original analysis by Pasini *et al.* are also being considered. We are interested in generalizing their results to include (a) arbitrary angle rotations and axes, (b) closed-system perturbative expansions about any value of ε , rather than only $\varepsilon = 0$, and (c) ε as a stochastic time-dependent variable/operator, which is relevant to previous work on decoherence control, e.g., [47].

ACKNOWLEDGEMENTS

MDG thanks Paul T. Boggs (SNL), and Robert L. Kosut (SC Solutions, Inc.) for illuminating discussions on control and nonlinear optimization. MDG and WMW thank Stefano Pasini and Götz S. Uhrig (Technische Universität Dortmund) for useful discussions regarding Ref. [7]. This work was supported by the Laboratory Directed Research and Development program at Sandia National Laboratories. Sandia is a multipurpose laboratory operated by Sandia Corporation, a Lockheed-Martin Company, for the United States Department of Energy under contract DE-AC04-94AL85000.

[1] F. Gaitan, *Quantum Error Correction and Fault Tolerant Quantum Computing* (CRC Press, 2008).

- [2] R. Liu, W. Yao, and L. J. Sham, *New J. Phys.* **9**, 226 (2007).
- [3] C. Brif, R. Chakrabarti, and H. Rabitz, *New J. Phys.* **12**, 075008 (Jul 2010).
- [4] G. S. Uhrig, *Phys. Rev. Lett.* **98**, 100504 (Mar 2007).
- [5] G. S. Uhrig, *New J. Phys.* **10**, 083024 (2008).
- [6] P. Karbach, S. Pasini, and G. S. Uhrig, *Phys. Rev. A* **78**, 022315 (2008); S. Pasini, T. Fischer, P. Karbach, and G. S. Uhrig, *ibid.* **77**, 032315 (Mar 2008); S. Pasini and G. S. Uhrig, *J. Phys. A: Math. and Theor.* **41**, 312005 (2008).
- [7] S. Pasini, P. Karbach, C. Raas, and G. S. Uhrig, *Phys. Rev. A* **80**, 022328 (Aug 2009).
- [8] S. Pasini and G. S. Uhrig, *J. Phys. A: Math. and Theor.* **43**, 132001 (2010).
- [9] A. Messiah, *Quantum Mechanics* (Dover Publications, Inc., New York, NY, 1999).
- [10] T. W. Borneman, M. D. Hürlimann, and D. G. Cory, *J. Magn. Res.* **207**, 220 (Dec 2010).
- [11] J. R. Petta, A. C. Johnson, J. M. Taylor, E. A. Laird, A. Yacoby, M. D. Lukin, C. M. Marcus, M. P. Hanson, and A. C. Gossard, *Science* **309**, 2180 (2005).
- [12] G. M. Huang, T. J. Tarn, and J. W. Clark, *J. Math. Phys.* **24**, 2608 (1983).
- [13] V. Ramakrishna, M. V. Salapaka, M. Dahleh, H. Rabitz, and A. Peirce, *Phys. Rev. A* **51**, 960 (Feb 1995).
- [14] R. Hanson, L. Kouwenhoven, J. Petta, S. Tarucha, and L. Vandersypen, *Rev. Mod. Phys.* **79**, 1217 (2007).
- [15] J. Taylor, J. Petta, A. Johnson, A. Yacoby, C. Marcus, and M. Lukin, *Phys. Rev. B* **76** (2007), doi:“bibinfo doi 10.1103/PhysRevB.76.035315”.
- [16] A. C. Johnson, J. R. Petta, J. M. Taylor, A. Yacoby, M. D. Lukin, C. M. Marcus, M. P. Hanson, and A. C. Gossard, *Nature* **435**, 925 (2005).
- [17] J. R. Petta, J. M. Taylor, A. C. Johnson, A. Yacoby, M. D. Lukin, C. M. Marcus, M. P. Hanson, and A. C. Gossard, *Physical Review Letters* **100**, 067601 (Feb 2008).
- [18] S. Foletti, H. Bluhm, D. Mahalu, V. Umansky, and A. Yacoby, *Nat. Phys.* **5**, 903 (Dec 2009).
- [19] H. Bluhm, S. Foletti, I. Neder, M. Rudner, D. Mahalu, V. Umansky, and A. Yacoby, “Long coherence of electron spins coupled to a nuclear spin bath,” (May 2010), <http://arxiv.org/abs/1005.2995>.
- [20] W. M. Witzel and S. D. Sarma, *Phys. Rev. B* **74**, 035322 (Jul 2006).
- [21] W. M. Witzel, X. Hu, and S. D. Sarma, *Phys. Rev B* **76**, 035212 (Jul 2007).
- [22] W. Yao, R. Liu, and L. J. Sham, *Phys. Rev. B* **74**, 195301 (Nov. 2006).

- [23] J. E. Levy, A. Ganti, C. A. Phillips, B. R. Hamlet, A. J. Landahl, T. M. Gurreri, R. D. Carr, and M. S. Carroll, in *Proceedings of the twenty-first annual symposium on parallelism in algorithms and architectures*, SPAA 2009 (ACM, New York, NY, USA, 2009) pp. 166–168.
- [24] W. M. Witzel, M. S. Carroll, A. Morello, L. Cywinacuteski, and S. D. Sarma, *Phys. Rev. Lett.* **105**, 187602 (Oct 2010).
- [25] R. de Sousa, *Phys. Rev. B* **76** (2007), doi:“bibinfo doi 10.1103/PhysRevB.76.245306.
- [26] M. D. Grace, J. Dominy, R. L. Kosut, C. Brif, and H. Rabitz, *New J. Phys.* **12**, 015001 (Jan 2010), Special Issue: Focus on Quantum Control.
- [27] M. Grace, C. Brif, H. Rabitz, I. A. Walmsley, R. L. Kosut, and D. A. Lidar, *J. Phys. B: At. Mol. Opt. Phys.* **40**, S103 (May 2007), Special Issue on the Dynamical Control of Entanglement and Decoherence.
- [28] C. A. Fuchs and J. van de Graaf, *IEEE Trans. Inf. Theory* **45**, 1216 (1999).
- [29] J. P. Palao and R. Kosloff, *Phys. Rev. A* **68**, 062308 (Dec 2003).
- [30] J. Dominy and H. Rabitz, *J. Phys. A: Math. and Theor.* **41**, 205305 (2008).
- [31] G. G. Balint-Kurti, S. Zou, and A. Brown, in *Adv. Chem. Phys.*, Vol. 138, edited by S. A. Rice (John Wiley & Sons, Inc., New York, NY, 2008) pp. 43–94.
- [32] V. Jurdjevic and H. J. Sussmann, *J. Diff. Eq.* **12**, 313 (1972).
- [33] C. Brif, R. Chakrabarti, and H. Rabitz, in *Adv. Chem. Phys.*, edited by S. A. Rice (John Wiley & Sons, Inc., New York, NY, 2010) (to be published).
- [34] W. H. Press, B. P. Flannery, S. A. Teukolsky, and W. T. Vetterling, *Numerical Recipes: The Art of Scientific Computing*, 2nd ed. (Cambridge University Press, Cambridge, 1992).
- [35] *Hybrid Metaheuristics: An Emerging Approach to Optimization*, edited by C. Blum, A. Roli, M. J. B. Aguilera, and M. Sampels (Springer-Verlag, Berlin, 2008).
- [36] E. Nielsen, R. W. Young, R. P. Muller, and M. S. Carroll, *Phys. Rev. B* **82**, 075319 (2010).
- [37] H. A. Rabitz, M. M. Hsieh, and C. M. Rosenthal, *Science* **303**, 1998 (2004).
- [38] T.-S. Ho, J. Dominy, and H. Rabitz, *Phys. Rev. A* **79**, 013422 (Jan 2009).
- [39] J. Dominy, T. Ho, and H. Rabitz, “Characterization of the critical sets of quantum unitary control landscapes,” (2011), <http://arxiv.org/abs/1102.3502>.
- [40] A. Rothman, T.-S. Ho, and H. Rabitz, *Phys. Rev. A* **72**, 023416 (2005); *J. Chem. Phys.* **123**, 134104 (2005); *Phys. Rev. A* **73**, 053401 (2006).
- [41] P. T. Boggs and J. W. Tolle, *Acta Numerica* **4**, 1 (1995).

- [42] V. Beltrani, J. Dominy, T.-S. Ho, and H. Rabitz, *J. Chem. Phys.* **126**, 094105 (2007).
- [43] R. Abraham, J. E. Marsden, and T. Ratiu, *Manifolds, Tensor Analysis, and Applications*, 2nd ed. (Springer-Verlag, New York, NY, 1988).
- [44] M. P. do Carmo, *Riemannian Geometry*, Mathematics: Theory & Applications (Birkhäuser, Boston, 1992).
- [45] J. W. Milnor, *Topology from a Differentiable Viewpoint*, Princeton Landmarks in Mathematics (Princeton University Press, Princeton, 1997).
- [46] K. Khodjasteh and D. A. Lidar, *Phys. Rev. A* **75**, 062310 (June 2007); K. Khodjasteh and L. Viola, *Phys. Rev. Lett.* **102**, 080501 (Feb 2009); *Phys. Rev. A* **80**, 032314 (Sep 2009); K. Khodjasteh, D. A. Lidar, and L. Viola, *Phys. Rev. Lett.* **104**, 090501 (Mar 2010).
- [47] K. C. Young, D. J. Gorman, and K. B. Whaley, “Fighting dephasing noise with robust optimal control,” (2010), <http://arxiv.org/abs/1005.5418>.

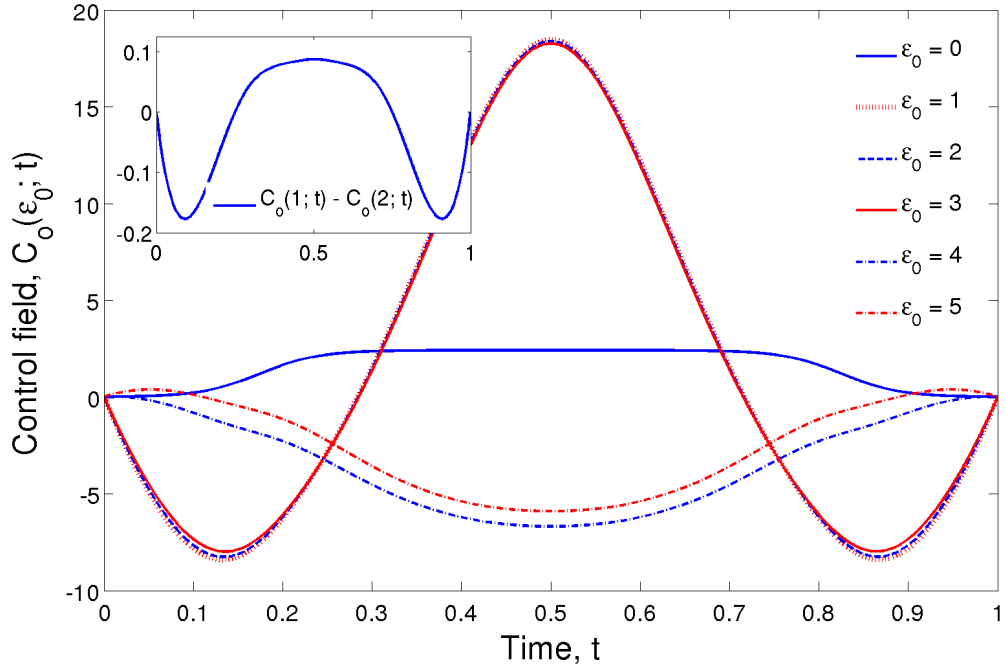


FIG. 1: OC fields producing a $Z_{\pi/2}$ operation for several *specific* values of ε_0 and $t_f = 1$ natural units. All OCs have distances $\Delta(Z_{\pi/2}, U_{t_f}) \leq 10^{-6}$. The inset presents the difference between $C_o(1; t)$ and $C_o(2; t)$. For the model DQD qubit described in section II, $C_o(\varepsilon_0; t) = 1$ corresponds to approximately 5.273×10^{-27} J or 3.291×10^{-8} eV.

FIGURES

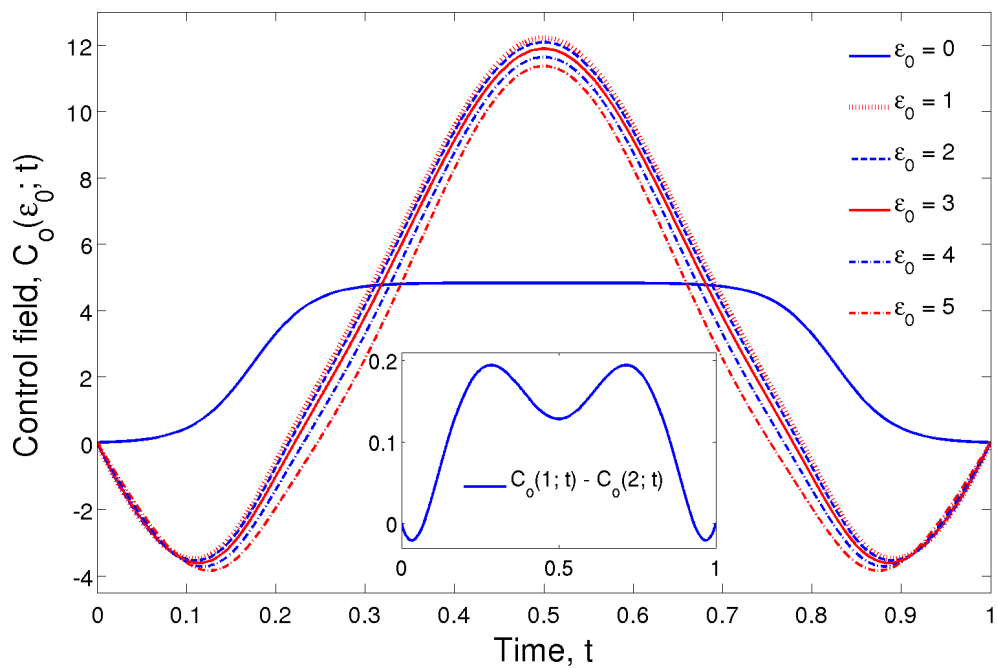


FIG. 2: OC fields producing a Z_π operation for several *specific* values of ε_0 and $t_f = 1$ natural units. All OCs have distances $\Delta(Z_\pi, U_{t_f}) < 10^{-6}$. The inset presents the difference between $C_o(1; t)$ and $C_o(2; t)$. For the model DQD qubit described in section II, $C_o(\varepsilon_0; t) = 1$ corresponds to approximately 5.273×10^{-27} J or 3.291×10^{-8} eV.

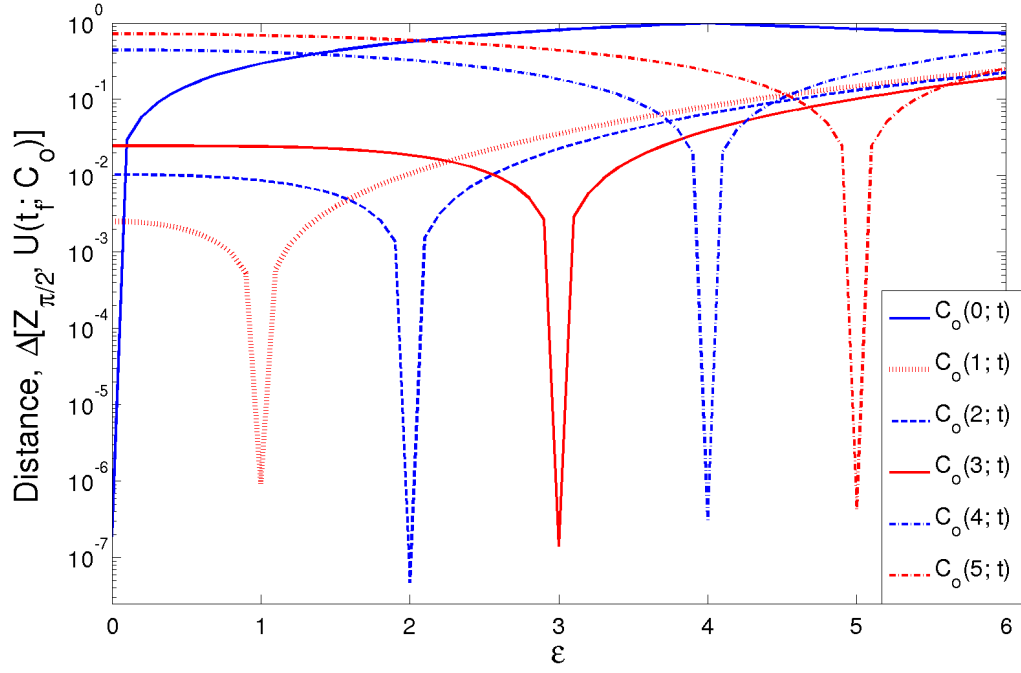


FIG. 3: Distance of OCs optimized with particular values of epsilon (solid blue circles), denoted as $C_o(\varepsilon_0; t)$, for the $Z_{\pi/2}$ operation [$\Delta(Z_{\pi/2}, U_{t_f}) < 10^{-6}$ for all controls], subsequently applied to a surrounding interval of ε .

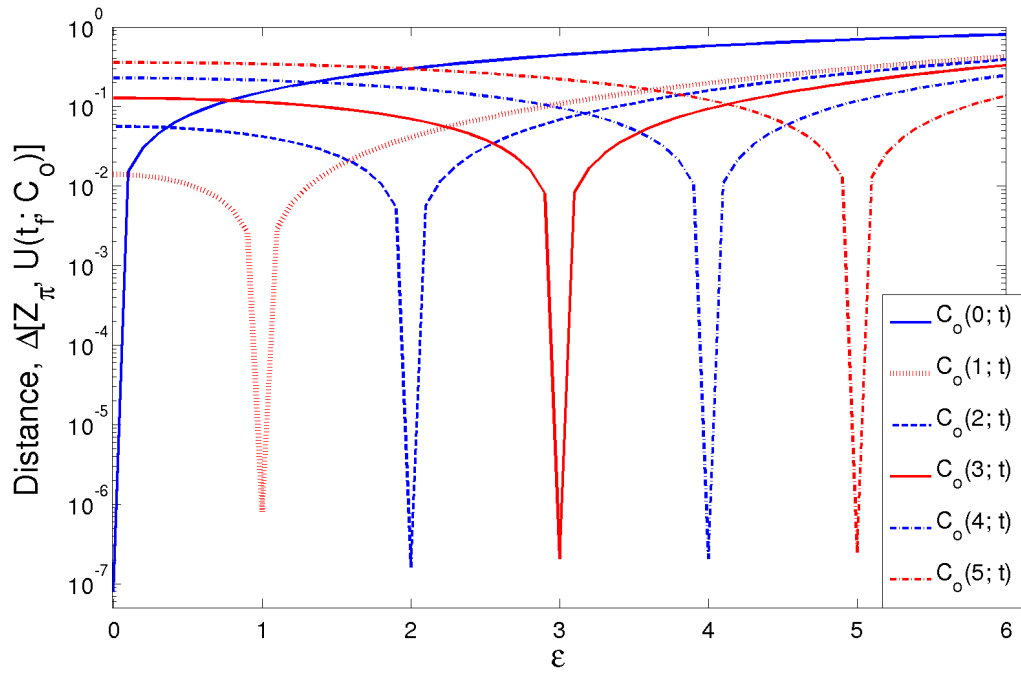


FIG. 4: Distance of OCs optimized with particular values of epsilon (solid blue circles), denoted as $C_o(\epsilon_0; t)$, for the Z_π operation [$\Delta(Z_\pi, U_{t_f}) < 10^{-6}$ for all controls], subsequently applied to a surrounding interval of ϵ .

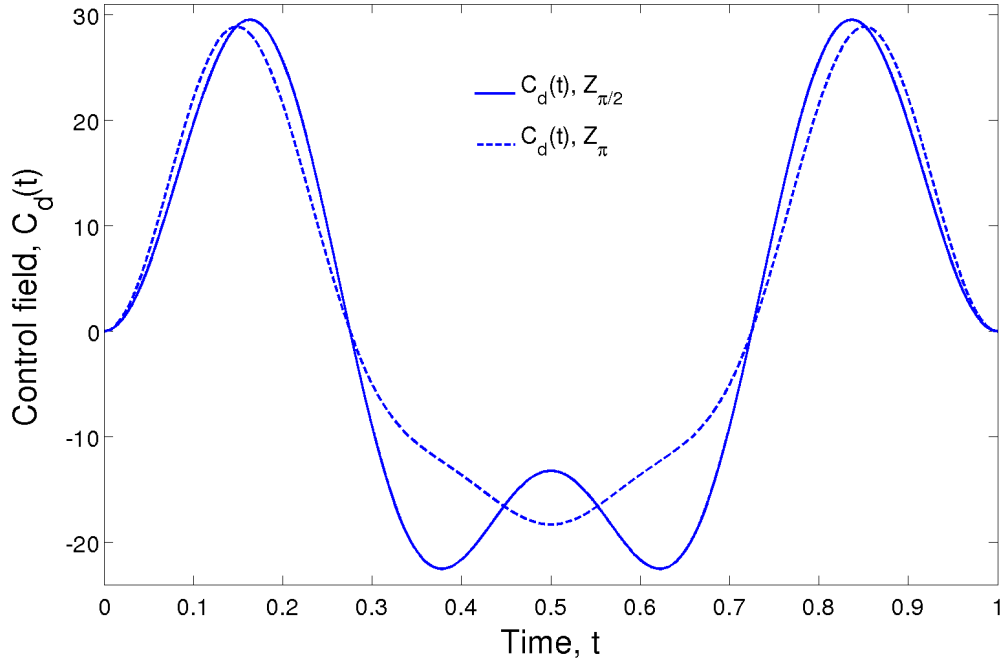


FIG. 5: Control fields $C_d(t)$ for $\pi/2$ - and π -rotations about the z -axis satisfying $\vec{\eta} = 0$, from Pasini *et al.* [7]. For the model DQD qubit described in section II, $C_d(t) = 1$ corresponds to approximately 5.273×10^{-27} J or 3.291×10^{-8} eV.

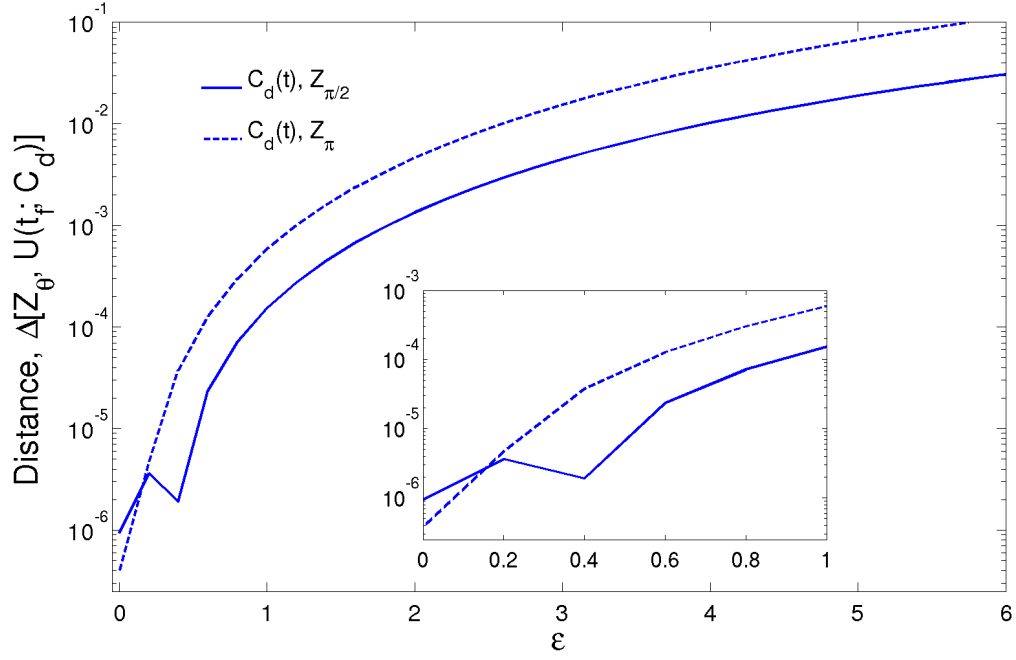


FIG. 6: Distance of the Z_θ operation as a function of ε and $\theta \in \{\pi/2, \pi\}$ for the Landau-Zener model of Eq. (1) and control fields $C_d(t)$ presented in Fig. 5. The inset displays the gate distance for $0 \leq \varepsilon \leq 1$ in greater detail.

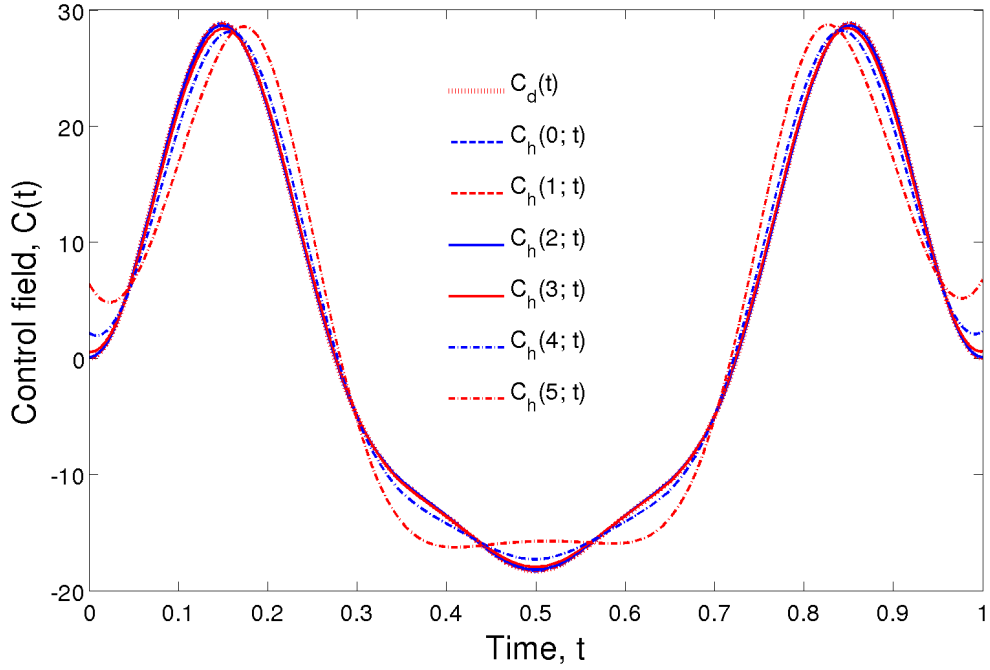


FIG. 7: DD+OC fields $C_h(\varepsilon_0; t)$ producing a Z_π operation, optimized using $C_d(t)$ as the initial control for all estimates/values of ε_0 and $t_f = 1$ natural units. For the model DQD qubit described in section II, $C_h(\varepsilon_0; t) = 1$ corresponds to approximately 5.273×10^{-27} J or 3.291×10^{-8} eV.

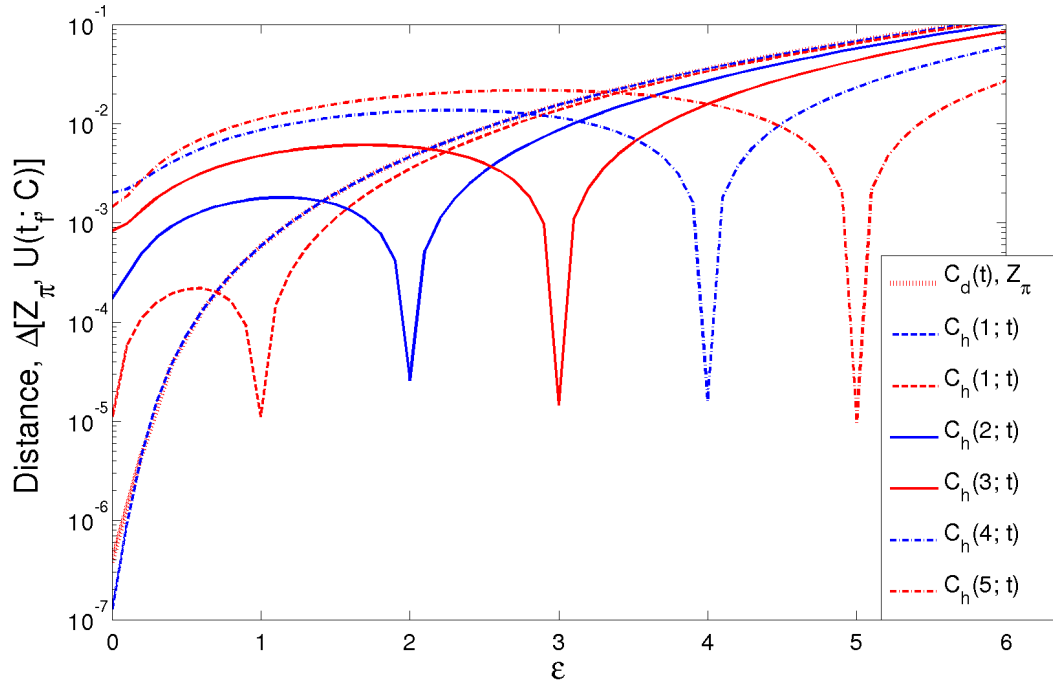


FIG. 8: Distance for the Z_π operation as a function of ε for control fields satisfying (a) $\vec{\eta} = 0$ (red dashed line) and (b) $\vec{\eta} \approx 0$ and $\Delta \approx 0$, optimized with a specified estimate/value of ε_0 .

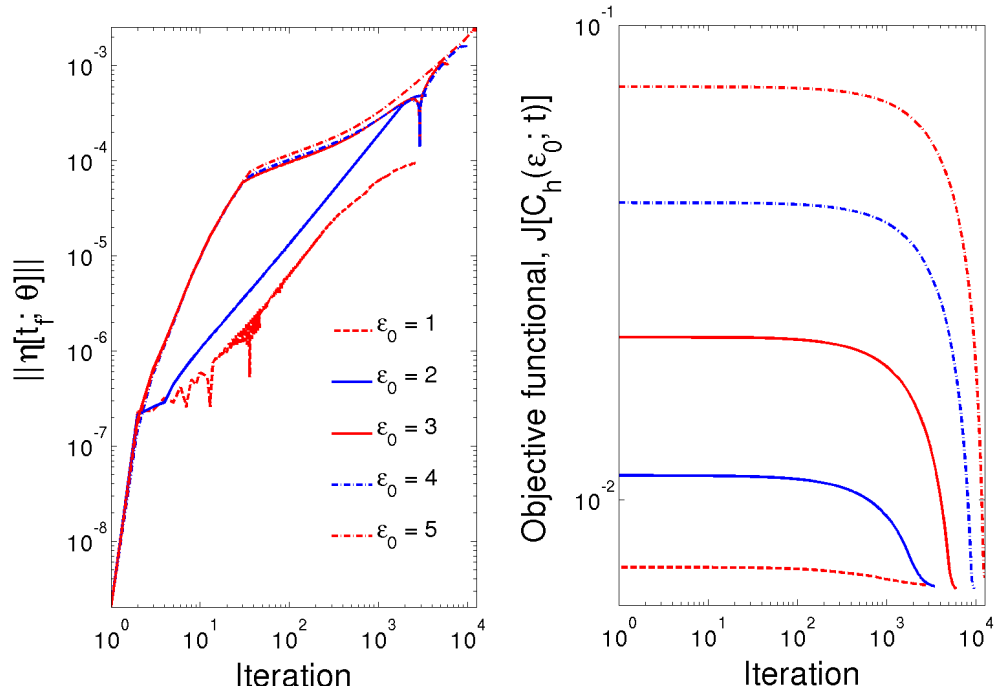


FIG. 9: $\|\eta\|$ and objective functional \mathcal{J} for the Z_π operation and each value of ϵ_0 considered, as a function of the number of DMORPH GrA optimization iterations.

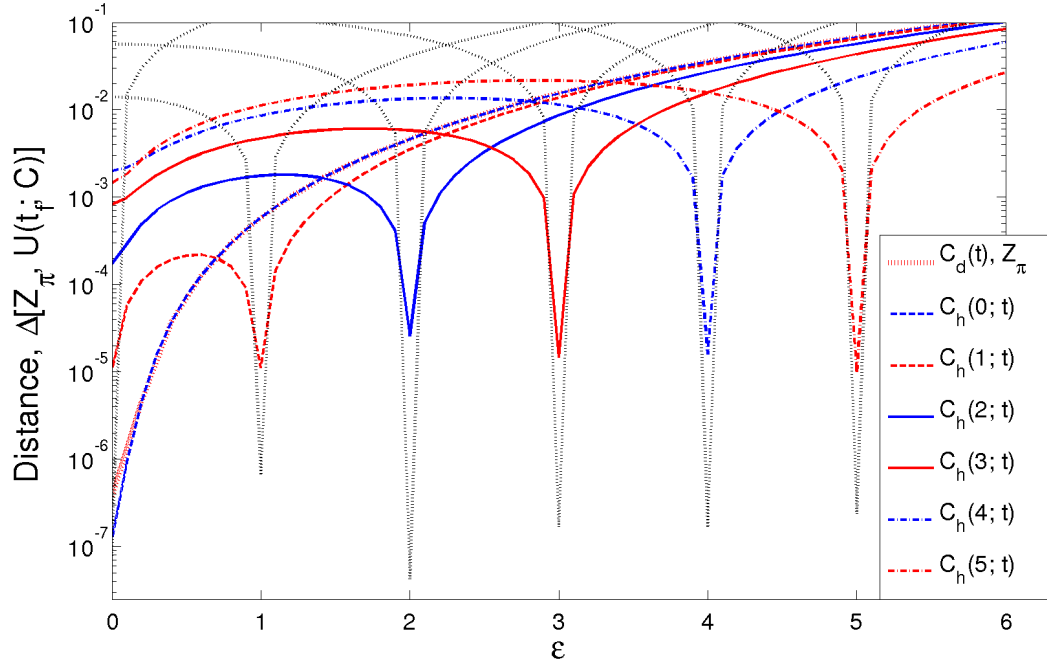


FIG. 10: Distance for the Z_π operation as a function of ε for control fields satisfying (a) $\vec{\eta} = 0$ (red dashed line), (b) $\vec{\eta} \approx 0$ and $\Delta \approx 0$, optimized with a specified estimate of ε_0 , and (c) results from $C_o(\varepsilon_0; t)$ in section IV (black dashed lines, from Fig. 4).

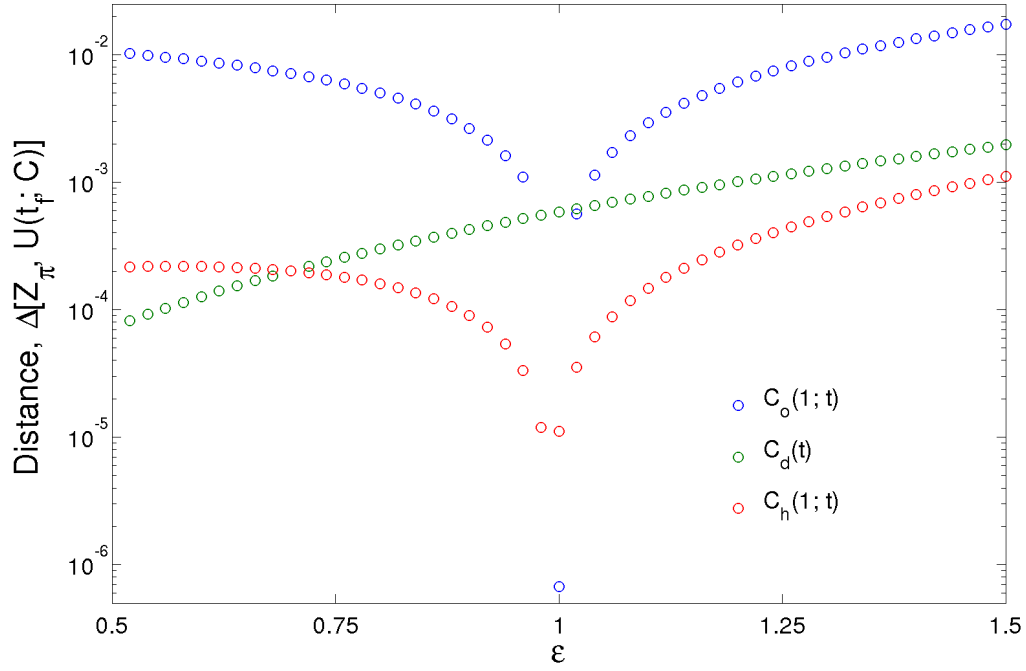


FIG. 11: Distance for the Z_π operation as a function of ε for $C_o(1; t)$, $C_d(t)$, and $C_h(1; t)$ controls in a unit interval centered at $\varepsilon_0 = 1$. Note that for $\varepsilon \geq 0.7$, $\Delta[Z_\pi, U(t_f; C_d)] \geq \Delta[Z_\pi, U(t_f; C_h)]$, i.e., $C_h(1; t)$ outperforms $C_d(t)$.

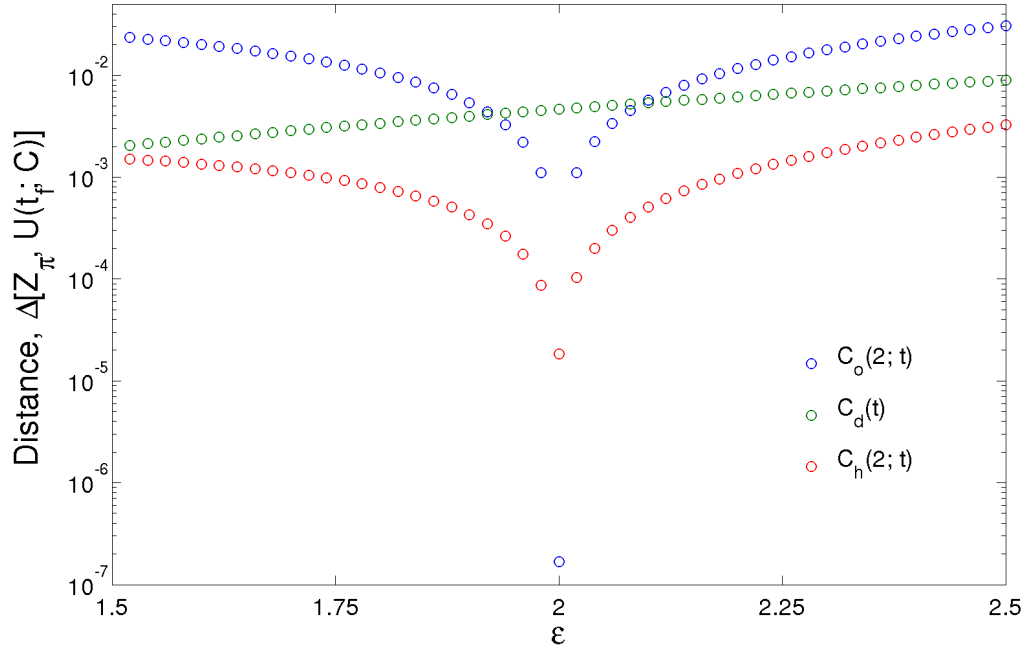


FIG. 12: Distance for the Z_π operation as a function of ε for $C_o(2; t)$, $C_d(t)$, and $C_h(2; t)$ controls in a unit interval centered at $\varepsilon_0 = 2$. Note that for $\varepsilon \geq 1.5$, $\Delta[Z_\pi, U(t_f; C_d)] \geq \Delta[Z_\pi, U(t_f; C_h)]$, i.e., $C_h(1; t)$ outperforms $C_d(t)$.